RSC Advances

PAPER

View Article Online
View Journal | View Issue

Cite this: *RSC Adv.*, 2015, **5**, 76116

Synthesis and electrochemical capacitance performance of polyaniline doped with lignosulfonate

Hailing Xu, Huang Jiang, Xingwei Li* and Gengchao Wang

Received 25th June 2015
Accepted 2nd September 2015

DOI: 10.1039/c5ra12292a

www.rsc.org/advances

Polyaniline doped with lignosulfonate (PANI/LGS) was prepared by using a facile oxidative polymerization of aniline with $(NH_4)_2S_2O_8$ as an oxidant, and the structure and morphology of PANI/LGS were investigated. As an active material for supercapacitors, the capacity retention rate of PANI/LGS was 75.1% with a growth of current density from 0.2 to 10 A g^{-1}, indicating a high rate performance, and that of PANI was only 38.3%. For PANI/LGS, a specific capacitance of 377.2 F g^{-1} remained at 10 A g^{-1}, and that of PANI was 183.7 F g^{-1}. Moreover, the cycling stability was also measured in a two-electrode symmetrical capacitor at a current density of 1.0 A g^{-1}. The capacity retention rate of PANI/LGS was 74.3% after 10 000 cycles, and that of PANI was 52.8%.

1. Introduction

Supercapacitors have gained great interest in energy storage devices on account of their fast charge/discharge rate and long term stability.[1,2] Pseudocapacitors are one family member of supercapacitors, which store charges through surface redox or faradaic reactions.[3] Typically, pseudocapacitive materials include transition metal oxides/hydroxides (MnO_2, $Ni(OH)_2$, $Co(OH)_2$, Co_3O_4) and conducting polymers.[4,5] Conducting polymers are interesting active materials because of their low cost, relatively high theoretical capacities, good conductivity and excellent environmental stability.[6] Among the conducting polymers used for this purpose, polyaniline (PANI) with unparalleled architectural diversity and flexibility, unique doping/de-doping mechanism and ease of preparation, is considered as one of the most suitable active materials for high performance supercapacitors.[7] However, its application is limited due to a high ion diffusion resistance and a big volumetric change in the doping/de-doping process, resulting in a low rate capability, a slow redox process and a poor cycling stability.[8]

It is found that the microstructure of electroactive polymers greatly influences their performances. Electroactive materials with nanostructures can provide large electroactive regions, shorten the path of ion diffusion and migration, and mitigate the mechanical deformation of electrode materials, which are benefit for increasing the utilization of active materials and improving their stability.[9,10]

A lot of dopants have also been used to afford PANI with ideal nanostructures, including organic acids, ions and metal.[11–17] For example, Bolagam *et al.* proposed that PANI doped with (cyclohexylamino)-1-propanesulfonic acid resulted in the formation of highly crystalline nanospheres with flake-like morphology.[11] Additionally, Bhandari *et al.* synthesized ultra-long hairy PANI nanowires *via* mechanochemical (solid state) polymerization method using $(NH_4)_2S_2O_8$ as an oxidant and citric acid as a dopant.[13]

It has been reported that some dopants stay in the polymer structure and other ones are kept into it during the electrochemical reduction/oxidation (it depends mainly on their size).[18–21] Such as, Shimidzu *et al.* prepared polypyrrole films with various electrolyte anions.[18] They found that the size of dopant anions influenced the oxidation–reduction process of polypyrrole. Very recently, Wu *et al.* developed PANI nanotubes doped with different organic acids, including malic acid (MA), propionic acid (PA), succinic acid (SA), tartaric acid (TA) and citric acid (CA), *via* a facile chemical soft template method.[21] And their electrochemical capacitance performances were characterized. As electrode materials, the specific capacitance of PANI-MA and PANI-CA nanotubes reached 658 F g^{-1} and 617 F g^{-1} at the current density of 0.1 A g^{-1} in 1.0 M H_2SO_4 electrolyte in a three-electrode cell. From their perspectives, the counter anion of surfactant can be trapped in the polymer matrix and the ion of electrolyte plays an important role in the redox process.

Natural polymeric acids and their derivatives, such as lignosulfonate,[22] have also been considered to be attracting dopants. As a by-product of the wood pulp industry, most of lignin and its derivatives are still "black liquor" directly into rivers, or are burned after concentrated. Theoretically, phenol groups in lignin can be further converted into quinone groups through the oxidation reaction, therefore lignin and its derivatives can also be

Shanghai Key Laboratory of Advanced Polymeric Materials, Key Laboratory for Ultrafine Materials of Ministry of Education, School of Materials Science and Engineering, East China University of Science and Technology, Shanghai 200237, P.R. China. E-mail: lixingwei_nj@yahoo.com; Fax: +86-21-64253527; Tel: +86-21-64253527

used for electrochemical energy storage.[23–27] Three main chemical structure of lignin before and after oxidation are as follows:[24]

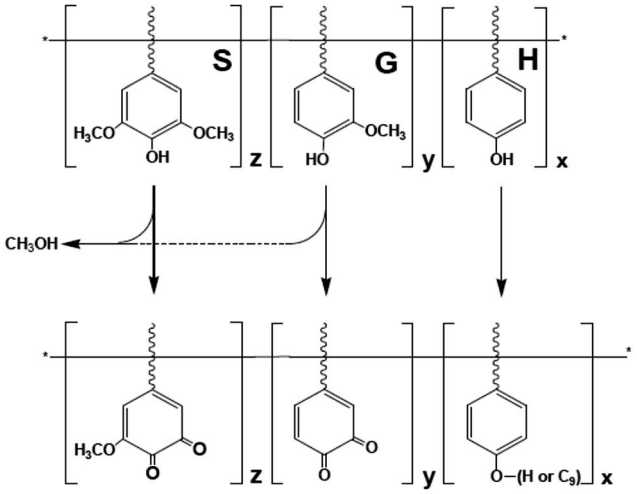

Obviously, the quinone group in lignin can be utilized for electron and proton storage and exchange during the redox cycling. However, lignin and its derivatives are chemically variable and electronically insulating.

Currently, there are some reports about lignin-based carbon materials for charge storages. Such as, Jin *et al.* fabricated carbon nanofibrous webs as a electrode for sodium ion batteries from polyacrylonitrile-refined lignin *via* eletrospinning followed by stabilization and carbonization.[28] Moreover, Lai *et al.* prepared lignin-based electrospun carbon nanofibers (ECNFs) with different mass ratio of lignin/polyvinyl alcohol (PVA) by first electrospinning mixtures containing alkali lignin together with polyvinyl alcohol (PVA) into composite nanofiber mats followed by stabilization in air and carbonization in an inert environment.[29] In a two-electrode cell, the specific capacitance of ECNFs (mass ratio of lignin/PVA: 70/30) was 64 F g^{-1} at 400 mA g^{-1} with the capacitance retention of 90% over 6000 cycles in 6.0 M KOH.

If lignin derivatives can be incorporated into an electrode material with good electronic and ionic conductivity, the redox function of phenol/quinone group is possible to be used for charge storages.[24,27] Therefore, combining conductive polymers and lignin derivatives has caused widespread concern. In addition to the work of O. Inganäs *et al.*,[24,27] Zhu *et al.* prepared polypyrrole/lignosulfonate coated cotton fabrics *via in situ* oxidation polymerization of pyrrole, and the specific capacitance of coated fabrics was measured in a two electrode cell, which its specific capacitance was 304 F g^{-1} at a charge/discharge current density of 0.1 A g^{-1} in 2.0 M NaCl.[25]

Since very little works reported PANI doped by LGS (PANI/LGS) for supercapacitors, we prepared PANI/LGS by the oxidative polymerization of aniline with $(NH_4)_2S_2O_8$ as an oxidant. And its electrochemical performances were investigated by cyclic voltammetry (CV), electrochemical impedance spectroscopic (EIS) and galvanostatic charge/discharge tests. Moreover, the effects of LGS on the capacitive performance of PANI had been analyzed in detail. As a result, PANI/LGS exhibited an excellent electrochemical performance and a superior cycling stability. This work suggests that the electrochemical performance of PANI can be improved by the doping of LGS.

2. Experimental section

2.1. Materials

Aniline (Shanghai Chemical Works, China) was distilled under reduced pressure before use. Lignosulfonate (LGS) was purchased from Aladdin Industrial Corporation and was used without further purification. Other chemicals used were of analytical reagent grade and were used as received. De-ionized water was used in this investigation.

2.2. Preparation of PANI/LGS

Synthesis of PANI/LGS was described below. First, 1.8 mL of aniline was dissolved in 150 mL of 1.5 M $HClO_4$ aqueous solution containing 0.3 g LGS with a constant stirring for 40 minutes. Then 4.56 g of $(NH_4)_2S_2O_8$ (dissolved in 50 mL of 1.5 M $HClO_4$ aqueous solution) was dropwise into the above system with a constant stirring. The polymerization was allowed to proceed for 24 hours at 0 °C. The product was filtered, and washed with de-ionized water until the filtrate became colorless and neutral. Finally, it was dried at 80 °C under vacuum for 24 hours to obtain PANI/LGS powder. In order to clarify the effects of LGS on the electrochemical performance of PANI, PANI was prepared as above, but without LGS.

2.3. Characterization of structure and morphology

The morphology was observed by a transmission electron microscopy (TEM, JEM-2100), and energy dispersive spectroscopy (EDS) was obtained. Fourier transform infrared spectra (FTIR) were recorded by using a Nicolet Magna-IR 550 spectrometer.

2.4. Conductivity and electrochemical measurements

Conductivity measurement was performed on the compressed pellets of powder by four-probe method at room temperature.

Cyclic voltammetry (CV), electrochemical impedance spectroscopy (EIS) and galvanostatic charge/discharge were measured by a CHI660D potentiostat/galvanostat. A conventional three-electrode cell was used, in which Pt and the saturated calomel electrodes were used as counter and reference electrodes, respectively. The electrolyte was 1.0 M H_2SO_4 aqueous solution. CV tests were carried out between −0.2 and 0.9 V *versus* the saturated calomel electrodes (SCE) at various scan rates of 16, 25, 36, 49, 64, 81 and 100 mV s^{-1}. EIS measurement was performed in a frequency range from 100 to 10 mHz at an open circuit potential with an AC amplitude of 5 mV. The charge/discharge measurements were carried out between 0 and 0.7 V. The specific capacitance was calculated from the charge/discharge curves according to the formula $C_m = C/m = I\Delta t/(m\Delta V)$, where C_m was the specific capacitance based on the mass of active materials (F g^{-1}), m was the mass of active material, I was charge/discharge current (A), Δt was the charge/discharge time (s), ΔV was the potential window (V). The cycling stability was measured on a LAND CT 2001A testing system at a current density of 1.0 A g^{-1}. A two-electrode

symmetrical capacitor was assembled with a thin polypropylene film as the separation.

In the qualitative CV measurements, the working electrode was prepared as follows: a certain amount of active materials was added into de-ionized water with ultrasonic dispersion for 30 minutes at room temperature. Then several drops of suspension were transferred to the surface of working electrode (Pt disk electrode of 2 mm diameter). A uniform film was formed after water evaporation, and thin film was rinsed with de-ionized water before used.

The working electrodes for electrochemical impedance spectroscopy, galvanostatic charge/discharge and cycling stability tests were prepared by mixing active material (PANI/LGS or PANI) with conductive carbon blacks (SUPERP™) and binder (polytetrafluoroethylene, PTFE) in a mass ratio of 85 : 10 : 5 and pressing onto titanium mesh at a pressure of 5 MPa. Each working electrode contained about 3 mg cm^{-2} of active material.

3. Results and discussion

3.1. Structure and morphology characterization

Fig. 1 displayed the FTIR spectra of PANI and PANI/LGS. From Fig. 1, it was found that PANI/LGS showed similar characteristic peaks as compared to those of PANI. For examples, the peaks centered at 1604 and 1476 cm^{-1} were attributed to the C=C stretching deformation mode of the quinoid and benzenoid rings in PANI, respectively, indicating the presence of emeraldine salts of PANI. The C–N stretching of the benzene ring occurred at 1309 cm^{-1}. The peak at 1135 cm^{-1} (–N–Q–N– stretching vibration) was also the characteristic peak of PANI, and the peak at 819 cm^{-1} was assigned to the out of plane bending vibration of C–H in the benzene ring.[30,31] In the spectrum of LGS, the peak at 3420 cm^{-1} was attributed to O–H. And C–H stretch in the methyl and methylene groups was in the range of 3000–2800 cm^{-1}. The strong peak at 1609 cm^{-1} was the C=C aromatic skeletal vibration, while the C–O stretching vibration appeared at 1215 cm^{-1}.[32,33] In comparison with PANI, some characteristic peaks of PANI/LGS had changed. Such as, the peaks around 1135, 1476 and 1604 cm^{-1} shifted to lower wave numbers (1109, 1464 and 1565 cm^{-1}), respectively. This result should be attributed to an interaction of PANI with LGS.[34]

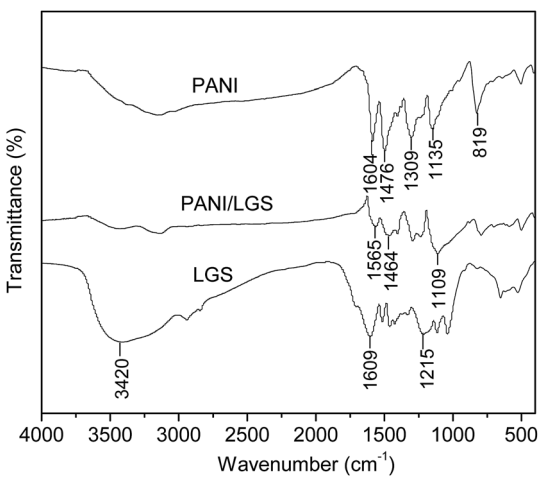

Fig. 1 FTIR spectra of PANI/LGS, PANI and LGS.

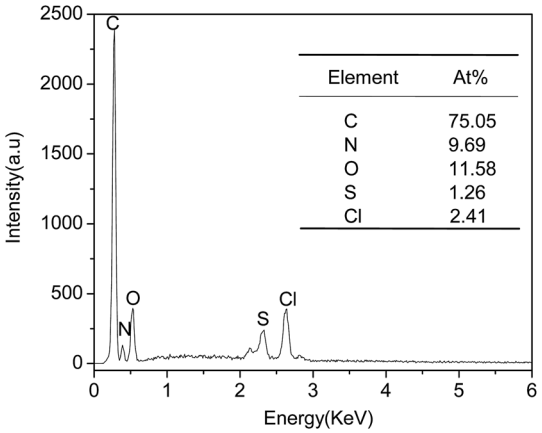

Fig. 2 EDS of PANI/LGS.

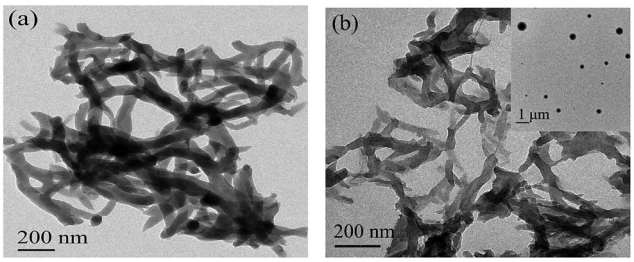

Fig. 3 TEM of PANI (a) and PANI/LGS (b) (the illustration was TEM of LGS).

The composition of PANI/LGS was also analyzed by EDS. As shown in Fig. 2, the S element was found in PANI/LGS, indicating the presence of LGS. Based on the result of EDS, the content of LGS was also estimated semi-quantitatively, which was about 20%.

TEM images of LGS, PANI and PANI/LGS were given in Fig. 3. Fig. 3a showed that the obtained PANI was nanofibers with a diameter of about 50 nm. However, the PANI/LGS showed a little different morphology in comparison with that of PANI (Fig. 3b). The diameter of PANI/LGS nanofibers was about 30 nm, and the boundaries between nanofibers became blurred, which might be due to the poor contrast or an almost molecular miscibility between the PANI and LGS.[24] The illustration in Fig. 3b displayed that LGS was granules, which was completely different from PANI and PANI/LGS. The above results showed that the morphology and structure of PANI were affected by the doping of LGS.

3.2. Conductivity and electrochemical performances

The conductivity of PANI/LGS was 2.41 S cm^{-1}, and that of PANI was 1.43 S cm^{-1}. Obviously, the conductivity of PANI was also improved by the doping of LGS.

Fig. 4 gave the CV curves of PANI, PANI/LGS and LGS at various scan rates. PANI showed two couples of redox peaks (O_1/R_1 and O_2/R_2), resulting in the pseudocapacitance. Among them, peaks O_1/R_1 were corresponding to the redox transition between leucoemeraldine (fully reduced) and emeraldine (half-oxidized), and peaks O_2/R_2 were ascribed to the transformation between emeraldine and pernigraniline (fully oxidized).[35] In CV curves of LGS, no redox peaks occurred, indicating a slow redox process due to a poor electrical conductivity. Obviously, CV curves of PANI/LGS were distinct from those of PANI. This meant that the introduction of LGS had a significant effect on the redox process of PANI, which should be ascribed to the contribution of LGS for electron and proton storage and exchange during the redox process of PANI.[24] Moreover, the presence of conducting PANI maybe also improved the redox function of phenol/quinone groups.

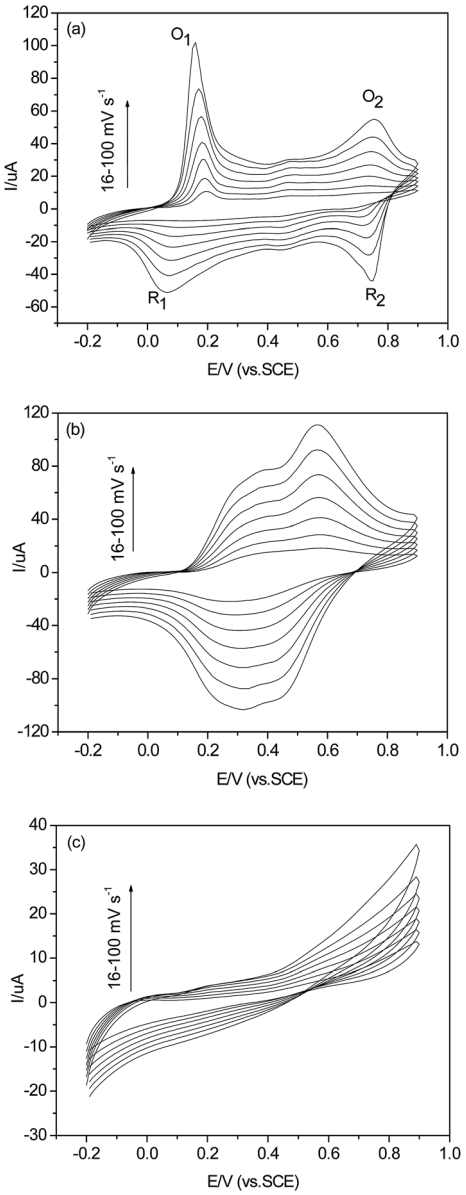

Fig. 4 CVs of PANI (a), PANI/LGS (b) and LGS (c).

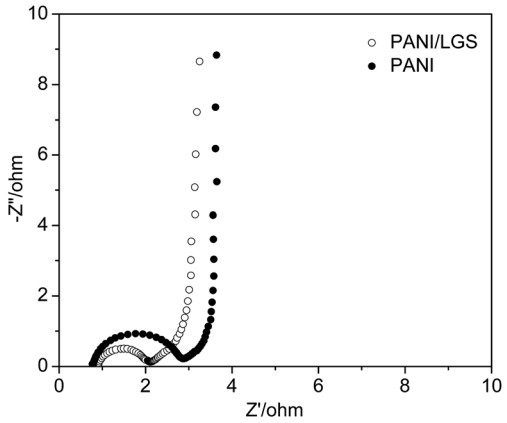

Fig. 5 EIS of PANI and PANI/LGS.

EIS of PANI/LGS and PANI were obtained at an open circuit potential, as shown in Fig. 5. These plots were all composed of three regions: a nearly vertical line at low frequency characterized capacitive behavior, a nearly 45° diagonal line at intermediate frequency related to diffusion resistance, and a semicircle at high frequency presented the charge transfer resistance.[36] Clearly, PANI/LGS showed a much smaller semi-circular line in the high frequency region, indicating a low resistance of interface charge transfer.

To understand the electrochemical performance of PANI/LGS, Fig. 6 displayed the charge/discharge curves of PANI/LGS and PANI at a current density of 1.0 A g^{-1} in 1.0 M H_2SO_4 aqueous solution. Compared with PANI, the charge/discharge curve of PANI/LGS electrode showed a quasi-triangular shape with a good symmetry, indicating a good electrochemical reversibility. In addition, it could be found that the PANI electrode had greater voltage drop (IR loss) than that of PANI/LGS electrode. At a current density of 1.0 A g^{-1}, the IR loss of PANI electrode was 0.1142 V, and that of PANI/LGS electrode was only 0.0059 V. Because the redox of phenol/quinone groups in the LGS can be utilized for electron and proton storage and

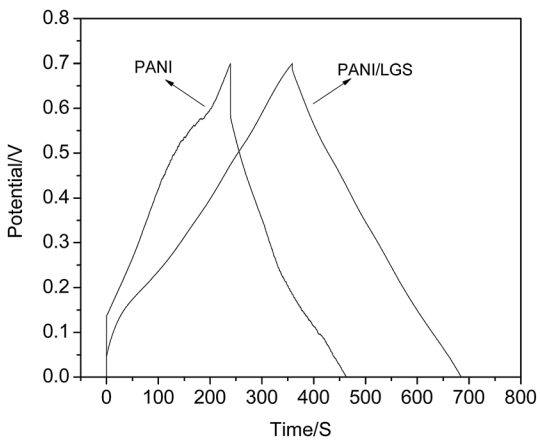

Fig. 6 The galvanostatic charge/discharge curves of PANI and PANI/LGS at a current density of 1.0 A g^{-1}, electrolyte: 1.0 M H_2SO_4 aqueous solution.

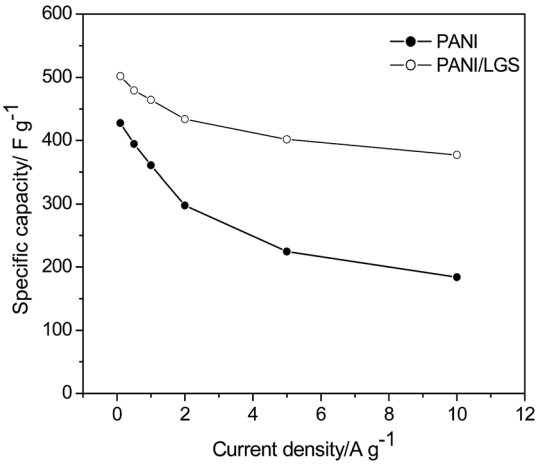

Fig. 7 The specific capacitance of PANI and PANI/LGS at different current densities, electrolyte: 1.0 M H_2SO_4 aqueous solution.

exchange, the synergy of conducting PANI and LGS enhances the electron transition in the charge/discharge process of PANI/LGS electrode, resulting in a low internal resistance.[24]

To further evaluate the electrochemical capacitance of PANI/LGS as an active material, the specific capacitance of PANI and PANI/LGS at different current densities (0.1, 0.5, 1.0, 2.0, 5.0, 10 A g^{-1}) was shown in Fig. 7. On increasing the current density from 0.1 to 10 A g^{-1}, the specific capacitance of PANI/LGS and PANI gradually decreased, which might be explained by the charge diffusion being too slow compared to the rapid increase in current density. It was noted that the specific capacitance of PANI/LGS was larger than those of PANI with the increase of the current densities. The specific capacitance of PANI/LGS decreased from 502.1 F g^{-1} at a current density of 0.1 A g^{-1} to 377.2 F g^{-1} at a current density of 10 A g^{-1}, which corresponded to a capacitance retention ratio of 75.1%, clearly higher than that (38.3%) of PANI, which the specific capacitance of PANI was only 183.7 F g^{-1} at a current density of 10 A g^{-1}. This result indicated that PANI/LGS had also a high rate performance.

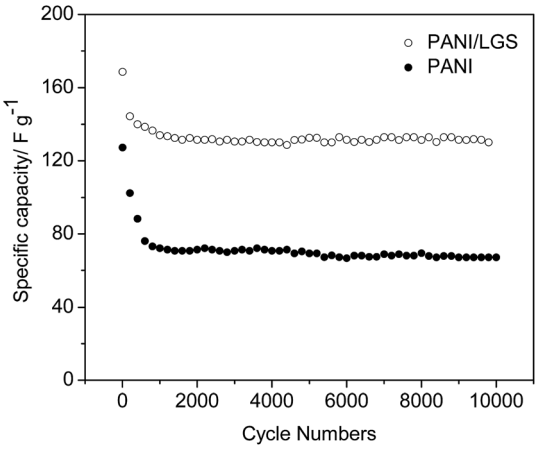

Fig. 8 The cycling stability of PANI/LGS and PANI assembled as symmetric supercapacitors at a current density of 1.0 A g^{-1} electrolyte: 1.0 M H_2SO_4 aqueous solution.

Cycling performance was important for practical applications. Therefore, the cycling stability of PANI/LGS and PANI electrodes were also measured at a current density of 1.0 A g^{-1} for 10 000 cycles in a two-electrode symmetrical capacitor. The specific capacitance as a function of cycle number was shown in Fig. 8. The specific capacitance of both electrodes decreased gradually with increasing cycle numbers. However, the capacitance retention of PANI/LGS was as high as 74.3% over 10 000 cycles, which was superior to that of PANI (52.8%). Good cycling performance of PANI/LGS should also be attributed to the doping of LGS. Some dopants, which stayed in the conducting polymer structure during the redox cycling, can improve the electrochemical stability of the conducting polymers.

4. Conclusions

In summary, PANI doped with LGS has been prepared by the oxidative polymerization of aniline in the presence of LGS. As an active material for supercapacitors, the capacity retention rate of PANI/LGS was 75.1% with a growth of current density from 0.1 to 10 A g^{-1}, and that of PANI was 38.3%. Even at a current density of 10 A g^{-1}, the specific capacitance of PANI/LGS still achieved 377.2 F g^{-1}, and that of PANI was 183.7 F g^{-1}. Furthermore, PANI/LGS obtained a capacity retention rate of 74.3% after 10 000 cycles at a current density of 1.0 A g^{-1}, which was 21.5% higher than that of PANI. The good electrochemical performance coupled with the convenient, economic and controlled preparation of PANI/LGS expands its potential application as an electrode material. There is still ample room for further developments to improve its electrochemical capacitance by searching through the universe of lignin. Moreover, our work also explores an easy method for the comprehensive utilization of black liquor of the wood pulp industry.

Notes and references

1 C. Ramasamy, J. Palma del Val and M. Anderson, *Electrochim. Acta*, 2014, **135**, 181–186.
2 B. Ravi, B. Rajender and S. Palaniappan, *J. Appl. Electrochem.*, 2015, **45**, 51–56.
3 K. V. Sankar and R. K. Selvan, *J. Power Sources*, 2015, **275**, 399–407.
4 S. H. Li, D. K. Huang, J. C. Yang, B. Y. Zhang, X. F. Zhang, G. Yang, M. K. Wang and Y. Shen, *Nano Energy*, 2014, **9**, 309–317.
5 L. Wang, Y. L. Zheng, S. L. Chen, Y. H. Ye, F. G. Xu, H. L. Tan, Z. Li, H. Q. Hou and Y. H. Song, *Electrochim. Acta*, 2014, **135**, 80–387.
6 H. L. Xu, X. W. Li and G. C. Wang, *J. Power Sources*, 2015, **294**, 16–21.
7 G. V. Ramana, P. S. Kumar, V. V. S. S. Srikanth, B. Padya and P. K. Jain, *J. Nanosci. Nanotechnol.*, 2015, **15**, 1338–1343.
8 Y. H. Jin and M. Q. Jia, *Colloids Surf., A*, 2015, **464**, 17–25.
9 L. Z. Fan, Y. S. Hu, J. Maier, P. Adelhelm, B. Smarsly and M. Antonietti, *Adv. Funct. Mater.*, 2007, **17**, 3083–3087.
10 J. Wei, J. Zhang, Y. Liu, G. Xu, Z. Chen and Q. Xu, *RSC Adv.*, 2013, **3**, 3957–3962.

11 R. Bolagam, R. Boddula and P. Srinivasan, *J. Appl. Electrochem.*, 2015, **45**, 51–56.
12 K. Pandey, P. Yadav and I. Mukhopadhyay, *Phys. Chem. Chem. Phys.*, 2015, **17**, 878–887.
13 S. Bhandari and D. Khastgir, *Mater. Lett.*, 2014, **135**, 202–205.
14 X. M. Lu, Q. F. Wu, H. Y. Mi and X. G. Zhang, *Acta Phys.–Chim. Sin.*, 2007, **23**, 820–824.
15 S. Palaniappan and S. L. Devi, *J. Appl. Polym. Sci.*, 2008, **107**, 1887–1892.
16 D. Ghosh, S. Giri, A. Mandal and C. K. Das, *RSC Adv.*, 2013, **3**, 11676–11685.
17 D. S. Patil, J. S. Shaikh, D. S. Dalavi, M. M. Karanjkar, R. S. Devan, Y. R. Ma and P. S. Patil, *J. Electrochem. Soc.*, 2011, **158**, A653–A657.
18 T. Shimidzu, A. Ohtani, T. Iyoda and K. Honda, *J. Electroanal. Chem.*, 1987, **224**, 123–135.
19 R. C. D. Peres, M. A. de Paoli and R. M. Torres, *Synth. Met.*, 1992, **48**, 259–270.
20 Y. F. Li and R. Y. Qian, *Synth. Met.*, 1988, **26**, 139–151.
21 W. L. Wu, D. Pan, Y. F. Li, G. H. Zhao, L. Y. Jing and S. L. Chen, *Electrochim. Acta*, 2015, **152**, 126–134.
22 G. Gupta, N. Birbilis and A. S. Khanna, *Int. J. Electrochem. Sci.*, 2013, **8**, 3132–3149.
23 S. V. Gnedenkov, D. P. Opra, S. L. Sinebryukhov, A. K. Tsvetnikov, A. Y. Ustinov and V. I. Sergienko, *J. Ind. Eng. Chem.*, 2014, **20**, 903–910.
24 G. Milczarek and O. Inganäs, *Science*, 2012, **335**, 1468–1471.
25 L. G. Zhu, L. Wu, Y. Y. Sun, M. X. Li, J. Xu, Z. K. Bai, G. J. Liang, L. Liu, D. Fang and W. L. Xu, *RSC Adv.*, 2014, **4**, 6261–6266.
26 S. Admassie, A. Elfwing, E. W. H. Jager, Q. Baod and O. Inganäs, *J. Mater. Chem. A*, 2014, **2**, 1974–1979.
27 D. H. Nagaraju, T. Rebis, R. Gabrielsson, A. Elfwing, G. Milczarek and O. Inganäs, *Adv. Energy Mater.*, 2014, **4**, 1–7.
28 J. Jin, S. J. Yu, Z. Q. Shi, C. Y. Wang and C. B. Chong, *J. Power Sources*, 2014, **272**, 800–807.
29 C. L. Lai, Z. P. Zhou, L. F. Zhang, X. X. Wang, Q. X. Zhou, Y. Zhao, Y. C. Wang, X. F. Wu, Z. T. Zhu and H. Fong, *J. Power Sources*, 2014, **247**, 134–141.
30 H. Hu, S. W. Liu, M. Hanif, S. L. Chen and H. Q. Hou, *J. Power Sources*, 2014, **268**, 451–458.
31 X. W. Li, X. H. Li, N. Dai, G. C. Wang and Z. Wang, *J. Power Sources*, 2010, **195**, 5417–5421.
32 N. E. Mansouri and J. Salvadó, *Ind. Crops Prod.*, 2007, **26**, 116–124.
33 Q. Shen, T. Zhang and M. F. Zhu, *Colloids Surf., A*, 2008, **320**, 57–60.
34 Z. He, Q. Lü and J. Zhang, *ACS Appl. Mater. Interfaces*, 2012, **4**, 369–374.
35 M. K. Park, K. Onishi, J. Locklin, F. Caruso and R. C. Advincula, *Langmuir*, 2003, **19**, 8550–8554.
36 A. Lewandowski, A. Olejniczak, M. Galinski and I. Stepniak, *J. Power Sources*, 2010, **195**, 5814–5819.